

# Iron-Chelating Drugs Enhance Cone Photoreceptor Survival in a Mouse Model of Retinitis Pigmentosa

Ke Wang,<sup>1</sup> Bo Peng,<sup>2</sup> Jia Xiao,<sup>3</sup> Orly Weinreb,<sup>4</sup> Moussa B. H. Youdim,<sup>4</sup> and Bin Lin<sup>5</sup>

<sup>1</sup>Guangdong-Hong Kong-Macau Institute of CNS Regeneration, Jinan University, Guangzhou, China

<sup>2</sup>Institute of Biomedical and Health Engineering, Shenzhen Institutes of Advanced Technology, Chinese Academy of Sciences, Shenzhen, China

<sup>3</sup>Department of Immunobiology, Institute of Tissue Transplantation and Immunology, Jinan University, Guangzhou, China

<sup>4</sup>Faculty of Medicine, Technion-Israel Institute of Technology, Haifa, Israel

<sup>5</sup>School of Optometry, The Hong Kong Polytechnic University, Kowloon, Hong Kong

Correspondence: Bin Lin, School of Optometry, The Hong Kong Polytechnic University, Hung Hom, Kowloon, Hong Kong; b.lin@polyu.edu.hk.

Moussa B. H. Youdim, Technion-Rappaport Family Faculty of Medicine, Technion-Israel Institute of Technology, Haifa, Israel; Youdim@tx.technion.ac.il.

Submitted: April 23, 2017

Accepted: September 10, 2017

Citation: Wang K, Peng B, Xiao J, Weinreb O, Youdim MBH, Lin B. Iron-chelating drugs enhance cone photoreceptor survival in a mouse model of retinitis pigmentosa. *Invest Ophthalmol Vis Sci.* 2017;58:5287–5297. DOI: 10.1167/iovs.17-22096

**PURPOSE.** Retinitis pigmentosa (RP) is a group of hereditary retinal degeneration in which mutations commonly result in the initial phase of rod cell death followed by gradual cone cell death. The mechanisms by which the mutations lead to photoreceptor cell death in RP have not been clearly elucidated. There is currently no effective treatment for RP. The purpose of this work was to explore iron chelation therapy for improving cone survival and function in the rd10 mouse model of RP.

**METHODS.** Two iron-chelating drugs, 5-(4-(2-hydroxyethyl) piperazin-1-yl (methyl)-8-hydroxyquinoline (VK28) and its chimeric derivative 5-(N-methyl-N-propargylaminomethyl)-quinoline-8-oldihydrochloride (VAR10303), were injected intraperitoneally to rd10 mice every other day starting from postnatal day 14. We investigate the effects of the two compounds on cone rescue at three time points, using a combination of immunocytochemistry, RT-PCR, Western blot analysis, and a series of visual function tests.

**RESULTS.** VK28 and VAR10303 treatments partially rescued cones, and significantly improved visual function in rd10 mice. Moreover, we showed that the neuroprotective effects of VK28 and VAR10303 were correlated to inhibition of neuroinflammation, oxidative stress, and apoptosis. Furthermore, we demonstrated that downregulation of NF- $\kappa$ B and p53 is likely to be the mechanisms by which proinflammatory mediators and apoptosis are reduced in the rd10 retina, respectively.

**CONCLUSIONS.** VK28 and VAR10303 provided partial histologic and functional rescue of cones in RD10 mice. Our study demonstrated that iron chelation therapy might represent an effective therapeutic strategy for RP patients.

**Keywords:** rd10 mice, iron-chelating drugs, photoreceptors, vision rescue, microglia

Retinitis pigmentosa (RP) is a genetically and phenotypically heterogeneous group of inherited retinal disorders. The most common forms of RP are caused by mutations in genes essential to rod photoreceptor function and metabolism, resulting in rod cell death and subsequent night blindness.<sup>1</sup> Cones that are present at a low density throughout the retina, with a sharp peak in the center of the fovea and represent 5% of all photoreceptors in the human eye,<sup>2–4</sup> do not express a mutated protein, and degenerate secondarily to rods. Although different approaches to treating retinal degeneration are being explored,<sup>5–10</sup> few effective treatments are currently available for RP patients. Therefore, establishing efficacious treatment strategies would create new perspectives for patients with retinal degeneration.

Growing evidence suggests that multiple mechanisms are involved in inducing photoreceptor cell death in RP.<sup>11,12</sup> Oxidative stress has previously been found to correlate with photoreceptor cell death in RP. Indeed, treatments with antioxidants showed a reduction in oxidative damage imposed by dying rods in the rd1 and rd10 mouse models of RP.<sup>7,13</sup> In addition, retinal iron accumulation is reported in RP animal

models.<sup>14,15</sup> Administration of iron chelators was shown to reduce iron-associated oxidative stress and attenuates photoreceptor degeneration in RP mouse models.<sup>16,17</sup> Moreover, neuroinflammation is reported to be associated with RP,<sup>18,19</sup> and activated microglia are observed in human RP patients and RP animal models.<sup>20–22</sup> Recently, we have shown that suppression of microglia activation promoted photoreceptor cell survival in the rd10 mouse model of RP,<sup>23</sup> confirming the involvement of neuroinflammation in RP progression. Furthermore, photoreceptor death is reported to be related to the downregulation of the mechanistic target of rapamycin pathway in RP mouse models.<sup>11</sup> Collectively, it appears that multiple mechanisms contribute to photoreceptor cell degeneration in RP.

Due to the complex pathology involved in RP progression, RP treatment poses a perplexing challenge. In this study, we explore iron chelation therapy in the rd10 mouse model of RP. To this end, we tested two iron-chelating compounds, 5-(4-(2-hydroxyethyl) piperazin-1-yl (methyl)-8-hydroxyquinoline (VK28) and its chimeric derivative 5-(N-methyl-N-propargylaminomethyl)-quinoline-8-oldihydrochloride (VAR10303), in the rd10 mouse. We have previously shown that VK28 and



VAR10303 exerted multiple effects including neuroprotection and neurorestoration in the animal models of Alzheimer and Parkinson's diseases.<sup>24-28</sup> VK28 has been shown to have neuroprotective activity against 6-hydroxydopamine and 1-methyl-4-phenyl-1,2,3,6-tetrahydropyridine (MPTP) neurotoxicity, iron accumulation, and microglial activation,<sup>27,29</sup> while VR10303 attenuates the apoptotic cascades (induction of B-cell lymphoma 2 [Bcl-2] and reduction of Bax), and increases the expression levels of Bcl-2, neurotrophic factors including brain-derived neurotrophic factor (BDNF) and glial cell line-derived neurotrophic factor (GDNF), and phosphorylation of Akt and Glycogen synthase kinase 3 (GSK-3 $\beta$ ).<sup>24-26</sup> Here, we have demonstrated that the two compounds provided significant histologic and functional rescue of photoreceptors and improved visual behaviors in rd10 mice.

## METHODS

### Animals and Drug Administration

Wild-type (WT; C57BL/6) mice, rd10 mice, and Cx3cr1<sup>GFP/GFP</sup> mice were obtained from Jackson Laboratory (Bar Harbor, ME, USA). Cx3cr1<sup>GFP/GFP</sup> mice were used to cross with WT (C57BL/6j) mice to obtain heterozygous Cx3cr1<sup>+GFP</sup> mice, and also to cross with rd10 mice to generate rd10/Cx3cr1<sup>+GFP</sup> mice, in which retinal microglia express green fluorescent protein (GFP) in a model of retinal degeneration. The littermates from Cx3cr1<sup>+GFP</sup> mice and rd10/Cx3cr1<sup>+GFP</sup> mice were used for the experiments. The genotypes of mouse litters were determined by PCR and confirmed by Southern blot analysis of genomic DNA from tail biopsies. Animals were bred and maintained at the Centralised Animal Facilities of The Hong Kong Polytechnic University on a 12-hour light-dark cycle with a room illumination of approximately 50 lux and water and food ad libitum. All experimental procedures were approved by the Animal Subjects Ethics Sub-Committee (ASESC) at The Hong Kong Polytechnic University and conducted in accordance with the ARVO Statement for the Use of Animals in Ophthalmic and Vision Research.

VAR10303 was synthesized by incorporating the neuroprotective N-propargyl moiety of the rasagiline into the antioxidant-iron chelator moiety of an 8-hydroxyquinoline derivative of VK28. VK28 or VAR10303 (5 mg/kg) was injected intraperitoneally to rd10 and rd10/Cx3cr1<sup>+GFP</sup> mice every other day, 48-hours apart, starting from postnatal day 14 (P14). Rd10 mice in control groups received the same volume of PBS (pH 7.4) at the same time points.

### Immunocytochemistry and Confocal Imaging

Mice were deeply anesthetized with a mixture of ketamine hydrochloride (30-40 mg/kg) and xylazine (3-6 mg/kg) at different time points. Retinas were dissected free of the vitreous and sclera in carboxygenated Ames' Medium (Sigma, St. Louis, MO, USA), and then fixed in 4% paraformaldehyde (PFA) in 0.1 M phosphate buffer, pH 7.4, for 0.5 to 1 hour. Some of retinas were sectioned serially at a thickness of 10 to 12  $\mu$ m using a cryostat. Both whole-mounted retinas and vertical sections were blocked in a solution containing 4% normal goat serum (NGS), 1% bovine serum albumin (BSA), and 0.3% Triton X-100 in PBS for 1 hour. Retinas were then incubated in a primary antibody from overnight to 5 days at 4°C. The following primary antibodies were applied: rabbit antibody to GFP (1:500; Invitrogen, Carlsbad, CA, USA), rat anti-mouse CD68 (1:500; AbD Serotec, Raleigh, NC, USA), and rabbit anti-red/green opsin (1:500; Chemicon, Temecula, CA, USA). After rinsing, a secondary antibody conjugated to either

Alexa 488 or Alexa 594 (1:500; Invitrogen) was applied for 2 hours at room temperature. Whole-mounted retinas and vertical sections were rinsed and cover slipped in Vectashield mounting medium (Vector Laboratories, Burlingame, CA, USA).

Confocal micrographs of fluorescent specimens from retinal whole-mounts and vertical sections were captured using a Zeiss LSM 700 Meta Axioplan 2 laser scanning confocal microscope (Carl Zeiss, Oberkochen, Germany) equipped with argon and helium-neon lasers. Plan-Apochromat  $\times 63/1.4$  or  $\times 40/1.4$  oil immersion objective lenses were used. Images scale was calibrated, and if necessary, brightness and contrast were adjusted using Photoshop CS3 software (Adobe Systems, San Jose, CA, USA).

### Data Analysis

For measurement of outer nuclear layer (ONL) thickness, some retinas were sectioned serially at a thickness of 10 to 12  $\mu$ m using a cryostat. Vertical sections passing through the optic nerve head were analyzed by counting the number of photoreceptor nuclei stained with diamidinophenylindole (DAPI). Two measurements were taken at 200  $\mu$ m (central region) and 1 mm (midperipheral region) from the optic nerve on both sides. Quantification of surviving cone photoreceptors was conducted in retinal whole-mounts, using a  $\times 40$  objective (numerical aperture: 0.85). Sampling areas were two fields of 240  $\times$  240- $\mu$ m squares along the dorsal-ventral axis of retinal whole-mounts, 1 mm (midperipheral region) from the optic nerve on both sides. Numbers of surviving cones were counted per grid directly under microscope or from z-stacked confocal images. The raw counts were then converted into cells/millimeter squared.

### Electroretinographic Analysis

Electroretinograms (ERGs) were recorded using an Espion ERG Diagnosys machine (Diagnosys, Littleton, MA, USA) as previously described by us.<sup>23</sup> In brief, flash ERG was measured using a gold wire corneal electrode, a forehead reference electrode, and a ground electrode near the tail. Scotopic, rod-mediated responses were obtained from dark-adapted animals at the following increasing light intensities: 0.01 and 3 cd-s/m<sup>2</sup>. Photopic, cone-mediated responses were performed following 10-minute light adaptation on the background light intensity of 30 cd/m<sup>2</sup>. Recordings were obtained at the light intensity of 3 cd-s/m<sup>2</sup>. From each animal, 15 waveforms were recorded and the values were averaged. The ERG b-wave amplitudes were measured from the trough of the a-wave to the peak of the first positive wave or, when the a-wave was not present, from baseline to the peak of the first positive wave.

### Optokinetic Tracking

Optokinetic tracking was performed as previously described by us.<sup>23</sup> Mice were placed on a platform positioned in the middle of an arena created by a quad-square of computer monitors. Vertical sine wave gratings (100% contrast) written in MATLAB (MathWorks, Natick, MA, USA) were projected on the computer monitors. The spatial frequencies tested were 0.05, 0.075, 0.1, 0.2, 0.3, 0.4, 0.5, 0.6 cycle per degree (cpd), at a constant speed of 12 degree per second. An infrared-sensitive small camera monitored the image of eye movements.

### ELISA Measurement

ELISA for TNF- $\alpha$  (cat no. 900-M54; PeproTech, Rocky Hill, NJ, USA), IL-6 $\beta$  (cat no. 900-K50; PeproTech), nuclear-factor kappa B (NF- $\kappa$ B) p65 (cat no. 7174C; Cell Signaling, Danvers, MA,

USA), caspase-3/7 (cat no. 13503; ATT Bioquest, Sunnyvale, CA, USA), caspase-8 (cat no. 22798; ATT Bioquest), hypoxia inducible factor (HIF)-1 $\alpha$  (cat no. DY1935-2; R&D Systems, Minneapolis, MO, USA), malondialdehyde (MDA; cat no. 21012; Oxis Research, Portland, OR, USA), reduced glutathione (GSH), and oxidized glutathione (GSSG) expression in retinas were performed using ELISA kits, respectively, according to manufacturer's instructions as previously described by us.<sup>23,30</sup>

Murine TNF- $\alpha$  ELISA development kit contains the key components required for the quantitative measurement of natural and/or recombinant murine TNF- $\alpha$  in a sandwich ELISA format. Mouse TNF- $\alpha$  is a glycoprotein composed of 156 amino acids produced mainly by monocytes and activated macrophages. The kit is recommended for assaying murine TNF- $\alpha$  (PeproTech).<sup>31,32</sup>

Murine IL-6 ELISA development kit contains the key components required for the quantitative measurement of natural and/or recombinant murine IL-6 in a sandwich ELISA format (manufacturer's technical information).<sup>31,33</sup>

Total NF- $\kappa$ B p65 Sandwich ELISA Kit is a solid phase sandwich ELISA kit that detects endogenous levels of total NF- $\kappa$ B p65 protein. The kit detects both the captured phospho- and nonphospho-NF- $\kappa$ B p65 protein (Cell Signaling).<sup>31</sup>

Caspase-3 Assay Kit uses (Z-DEVD)2R110 as fluorogenic indicator for assaying caspase-3 activity. Cleavage of R110 peptides by caspases generates strongly fluorescent R110 that can be monitored fluorimetrically at 510 to 530 nm with excitation of 488 nm, the most common excitation light source used in fluorescence instruments. This kit can be used to continuously measure the activities of caspase 3 and 7 in cell extracts and purified enzyme preparations using a fluorescence microplate reader or fluorometer (ATT Bioquest).<sup>31</sup>

Caspase 8 Activity Apoptosis Assay Kit is designed to monitor cell apoptosis by measuring caspase 8 activity. This kit uses (Ac-IETD)2-R110 as a fluorogenic indicator for caspase 8 activity. Cleavage of rhodamine 110 (R110) peptides by caspase 8 generates strongly fluorescent R110, which is monitored at the emission between 520 and 530 nm with the excitation between 480 and 500 nm (ATT Bioquest).<sup>31</sup>

The Human/Mouse Total HIF-1 $\alpha$  DuoSet IC ELISA kit contains the basic components required for the development of sandwich ELISAs to measure in cell lysates. The kit's specificity for recognizing HIF-1 $\alpha$  was demonstrated by Western blot analysis. An immobilized capture antibody specific for binds both phosphorylated and unphosphorylated (R&D Systems).<sup>31</sup>

## Western Blotting Analysis

CD68 (cat no. sc-7084; Santa Cruz Biotechnology, Santa Cruz, CA, USA), phospho-inhibitor of nuclear factor- $\kappa$ B (I $\kappa$ B) $\alpha$  (cat no. 2859; Cell Signaling), I $\kappa$ B $\alpha$  (cat no. 9247; Cell Signaling), nuclear p53 (cat no. 2524; Cell Signaling), phospho-p53 (cat no. 9284; Cell Signaling), and transferrin (cat no. sc-52256; Santa Cruz Biotechnology) proteins were detected by Western blotting as previously described by us.<sup>23,30</sup> Protocols for cytosolic and nuclear protein extraction were performed as previously described by us.<sup>34</sup> Briefly, following homogenization, retinas were lysed for 30 minutes on ice in RIPA buffer (Sigma-Aldrich) supplemented with protease inhibitors. Proteins were quantified using a BCA Protein Assay Kit. The samples were loaded onto polyacrylamide bis-tris gels and then transferred to nitrocellulose membrane for Western blot. After blocking, membranes were incubated with primary antibodies followed by secondary antibodies. The ratio of the optical density of the protein product to the internal control ( $\beta$ -actin, cat no. 37001 Cell Signaling) was obtained and was expressed as ratio or percentage of the control value in the Figures.

CD68 is a membrane glycoprotein present in lysosomes of macrophage-lineage cells<sup>35</sup>; the antibody used in this study is an affinity purified goat polyclonal antibody raised against a peptide mapping near the C-terminus of CD68 of mouse origin, and recognizes on Western blot a protein of 75 to 110 kDa specifically present in tissue macrophages that correspond to different degrees of protein glycosylation related to cell activation and phagocytosis.<sup>34,36</sup>

Phospho-I $\kappa$ B $\alpha$  is a rabbit monoclonal antibody (clone 14D4) and produced by immunizing animals with a synthetic phosphopeptide corresponding to residues surrounding Ser32 of human I $\kappa$ B $\alpha$ . Phospho-I $\kappa$ B $\alpha$  detects endogenous levels of I $\kappa$ B $\alpha$  only when phosphorylated at Ser32. This Phospho-I $\kappa$ B $\alpha$  antibody recognizes a single band of 40-kDa by Western blot of extracts from HeLa and NIH/3T3 cells and mouse tissues (Cell Signaling).<sup>34,37</sup>

The I $\kappa$ B $\alpha$  antibody is a mouse monoclonal antibody to 112B2 to NF $\kappa$ BIA, and nuclear factor of kappa light polypeptide gene enhancer in B-cells inhibitor, alpha. The I $\kappa$ B $\alpha$  antibody is produced by immunizing animals with a synthetic peptide corresponding to residues near the carboxy-terminus of human I $\kappa$ B $\alpha$ . The monoclonal antibody detects endogenous levels of total I $\kappa$ B $\alpha$  protein and recognizes a single band of 39-kDa by Western blot of extracts from HeLa cells and mouse livers (Cell Signaling).<sup>30</sup>

Nuclear p53 antibody is produced by immunizing animals with a synthetic peptide corresponding to residues surrounding Ser20 of human p53. p53 immunoreactivity detected with this antibody is exclusively nuclear. This antibody is highly specific for detecting a major protein band at 53 kDa that has the same mobility as recombinant p53 (Cell Signaling).<sup>38</sup>

Phospho-p53 antibody is a polyclonal antibody and produced by immunizing animals with a synthetic phosphopeptide corresponding to residues surrounding Ser15 of human p53. This antibody detects endogenous levels of p53 only when phosphorylated at serine 15.<sup>38</sup> This antibody does not cross-react with p53 phosphorylated at other sites and recognizes a single band of 53-kDa by Western blot of extracts from MvILu cells (Cell Signaling).

Transferrin antibody (11D3) is a mouse monoclonal antibody, raised against placental transferrin receptor or transferrin of human origin, and is recommended for detection of transferrin of mouse, rat, and human origin by Western blotting. The antibody recognizes a band of approximately 72-kDa by Western blot analysis of extracts from Hep G2 whole cell and rat sympathetic neurons (Santa Cruz Biotechnology).<sup>39</sup>

## Statistical Analysis

Data were represented as means  $\pm$  SDs. ANOVAs with Bonferroni's and Dunnett's post hoc tests for multiple comparisons were performed with Origin (OriginLab, Wellesley Hills, MA, USA). Software programs written in MATLAB on full data sets were used to detect significant differences in the means. A *P* value less than 0.05 was considered statistically significant.

## RESULTS

### VK28 and VAR10303 Partially Rescued Photoreceptor Morphology in the rd10 Mouse Retina

Rd10 mice are a well-characterized mouse model of RP, in which a mutation of the beta subunit of rod-specific phosphodiesterase (PDE6 $\beta$ ) gene causes the massive degeneration of rod photoreceptors followed by cone photoreceptors.<sup>40</sup> Mutations of the same gene have been linked to some

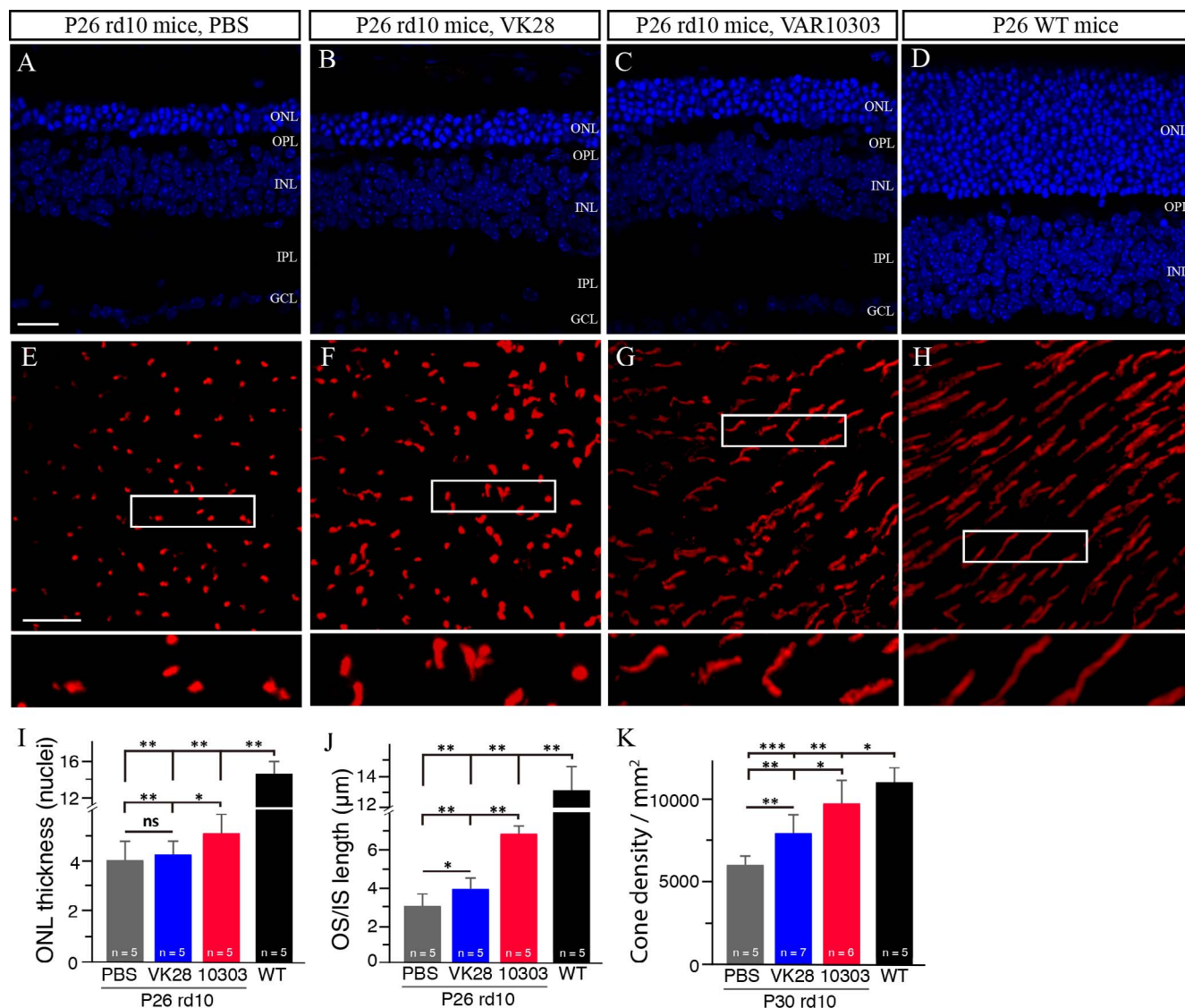


**FIGURE 1.** VK28 and VAR10303 partially rescue cone morphology in the rd10 mouse retina. (A–D) The nuclear layers in retinal sections were stained with DAPI (blue). Progressive thinning of the ONL is observed in rd10 retina (A) blue, while VK28 (B) and VAR10303 (C) preserved the thickness of the ONL. Retinas from WT mice at the same age are used as a comparison (D). (E–H) Confocal images of retinal whole-mounts of P26 rd10 mice following 12-day treatments with PBS (E), VK28 (F), or VAR10303 (G). Retinas from P26 WT mice are used as a comparison (H). The OSs of cone photoreceptors were detected by an antibody against red/green opsin (red). Illustration of highly magnified images from the boxed regions indicated above, respectively. (I) Plot of the ONL thickness from P26 mice measured in numbers of photoreceptor nuclei per column. (J) Plot of the length of OS/ISs measured in retinal sections of P26 mice. The OS/ISs of cones were revealed by an antibody against red/green opsins. (H) Quantification of cone densities from P30 rd10 mice following 16-day drug treatments. Results are presented as means  $\pm$  SDs and were analyzed using the Student's *t*-test. ns, not significant; \**P* < 0.05, \*\**P* < 0.01, and \*\*\**P* < 0.001. Scale bars: 20  $\mu$ m. ONL, outer nuclear layer; OPL, outer plexiform layer; INL, inner nuclear layer; IPL, inner plexiform layer; GCL, ganglion cell layer; OS, outer segment; IS, inner segment; n, number of mice in each group.

forms of human RP.<sup>41</sup> Rod degeneration begins around P18 and the peak of photoreceptor degeneration is reached at P25 in the rd10 mouse retina.<sup>42,43</sup> Because of the late initiation and mild degeneration, the rd10 mouse is increasingly being used for research to develop new experimental therapies for RP. We treated rd10 mice with VK28 or VAR10303 starting from P14, which is a few days earlier before the initiation of rod degeneration, and performed morphologic analysis at P26 and P30.

To assess the effectiveness of VK28 and VAR10303 on rod survival, the numbers of photoreceptor nuclei (97% of photoreceptor nuclei in the ONL of the mouse retina are rods<sup>44</sup>) were counted in retinal vertical sections. At P26, the

ONL in rd10 mice contained 3 to 5 rows of photoreceptor nuclei, while 14 to 16 rows were observed in normal WT mice (*P* < 0.01; Figs. 1A, 1D, 1I). Compared with rd10 controls, VAR10303-treated eyes had a thicker ONL (*P* < 0.05; Figs. 1C, 1I), indicating the reduction of rod cell death in VAR10303-treated rd10 mice. A thicker ONL was also observed in VK28-treated rd10 mice compared with rd10 controls (*P* > 0.05; Figs. 1B, 1I).

To characterize the protective effect of VK28 and VAR10303 on cone photoreceptors, we labeled whole-mounted rd10 retinas with an antibody specific for red/green cone opsins, and studied cone morphology and quantified cones (Figs. 1E–H). Cones in WT mouse retinas show

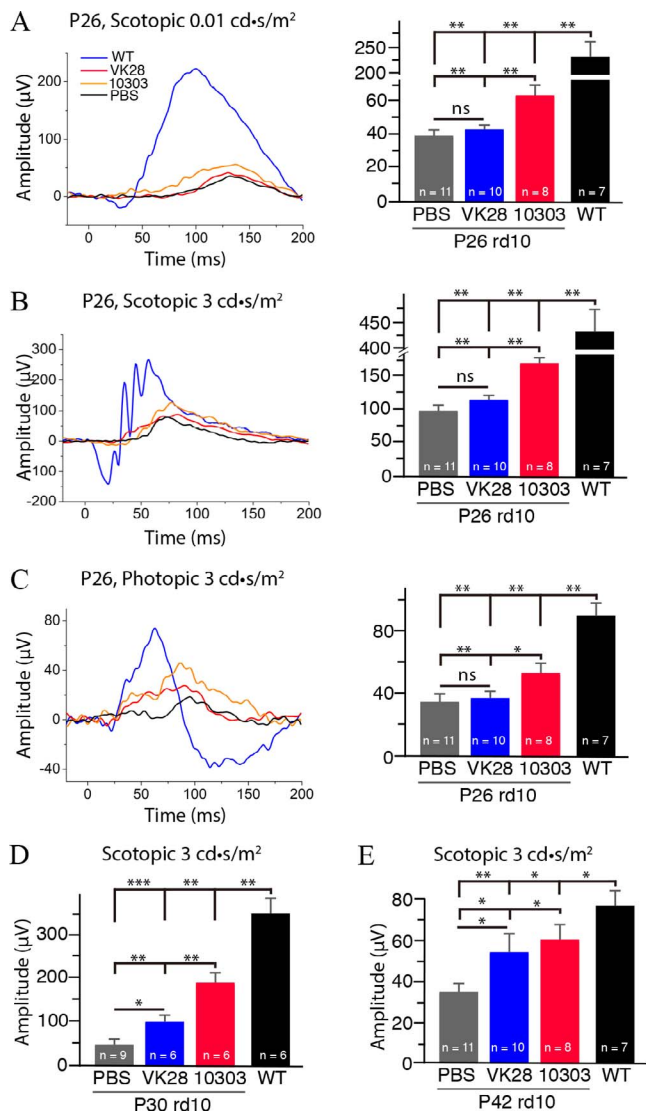


**FIGURE 2.** VK28 and VAR10303 partially rescue photoreceptor function in the rd10 mouse retina. (A, B) Representative scotopic ERG responses to 0.01- and 3-cd·s/m<sup>2</sup> light intensities from P26 rd10 mice treated with PBS, VK28, or VAR10303 from P14 to P25. Scotopic ERG responses from C57BL/6 (blue curve) are shown as comparisons. Average scotopic b-wave amplitudes elicited at both 0.01- and 3-cd·s/m<sup>2</sup> light intensities are shown on the right panel. Data are expressed as the mean ± SD. (C) Representative photopic ERG responses to 3-cd·s/m<sup>2</sup> light intensity from P26 rd10 mice are on the left, and averaged photopic b-wave amplitudes elicited at 3-cd·s/m<sup>2</sup> light intensity are on the right. (D) Average scotopic b-wave amplitudes elicited at 3-cd·s/m<sup>2</sup> light intensity were from P30 rd10 mice treated with PBS, VK28, or VAR10303 from P14 to P29. (E) Average scotopic b-wave amplitudes elicited at 3-cd·s/m<sup>2</sup> light intensity were from P42 rd10 mice treated with PBS, VK28, or VAR10303 from P14 to P41. Values are means and SDs and were analyzed using the Student's *t*-test. \**P* < 0.05 and \*\**P* < 0.01. ns, not significant; n, number of mice in each group.

elongated outer segments (OS) (Fig. 1H), while cones in PBS-treated P26 rd10 mouse retinas displayed shortened and fragmented OSs (Fig. 1E). VK28 and VAR10303 treatments partially preserved cone OSs, which maintained elongated shapes, in P26 rd10 retinas (Figs. 1E, 1G). Qualification of cone OS/IS length in retinal vertical sections showed that cone OS/IS length were largely preserved in VAR10303-treated P26 rd10 retinas (*P* < 0.01; Fig. 1J), and partially saved in the VK28-treated P26 rd10 retina (*P* < 0.05; Fig. 1J), when

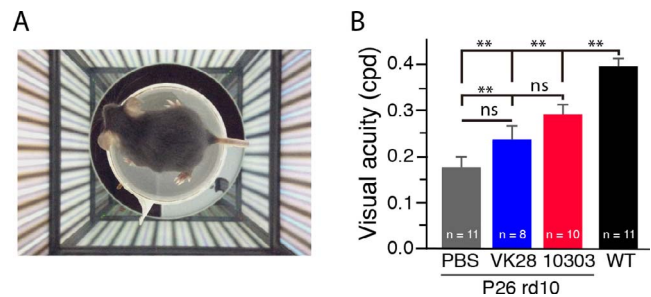


**FIGURE 3.** VK28 and VAR10303 improved visual acuity in rd10 mice. Photopic visual acuity was measured by the optokinetic response under light-adapted condition. (A) A single-frame video camera image of a mouse surrounded by 360° of sine wave gratings. (B) Average visual acuity was evaluated from P26 rd10 mice following treatments with PBS, VK28, or VAR10303. Results are presented as means ± SDs and were analyzed using the Student's *t*-test. \*\**P* < 0.01. ns, not significant; n, number of mice in each group.

compared with age-matched rd10 controls. At P26, average cone density was comparable among PBS- and VK28- and VAR10303-treated rd10 retinas and WT retinas (data not shown). However, there was a substantial loss of cone photoreceptors in PBS-treated P30 rd10 retinas when compared with age-matched WT (*P* < 0.001; Fig. 1K). Treatments with VK28 or VAR10303 enhanced cone survival in rd10 retinas, with average density of cones markedly higher than PBS-treated P30 rd10 retinas (*P* < 0.01; Fig. 1K). Taken together, two iron-chelating drugs provided significant histologic rescue of cones in rd10 mice.

### VK28 and VAR10303 Partially Rescued Photoreceptor Function in the rd10 Retina

Functional rescue of photoreceptors in drug-treated rd10 mice were monitored by ERG. Because a-waves were variable and small and couldn't be measured reliably, we thus chose b-waves as an indirect measure of photoreceptor function for the comparison of visual function. Representative ERG recordings are shown in Figure 2. Following a 12-day treatment, we observed markedly increased amplitudes of scotopic b-wave in P26 rd10 mice receiving VAR10303 treatment, compared with PBS-treated rd10 controls (*P* < 0.01; Figs. 2A, 2B). Similarly, photopic ERG b-wave amplitudes were significantly larger in VAR10303-treated rd10 mice than in PBS-treated rd10 controls (*P* < 0.01; Fig. 2C), suggesting improved retinal function. On the other hand, VK28 didn't show any obvious effects on the functional rescue of photoreceptors under both scotopic and photopic conditions at P26 (*P* > 0.05; Figs. 2A–C). However, the protective effect of VK28 became prominent following the long-time treatment with VK28. Scotopic b-wave amplitudes were significantly higher in VK28-treated P30 and P42 rd10 mice, compared with age-matched PBS-treated rd10 controls (*P* < 0.05; Figs. 2D–E), indicating a better retinal function rescue. Similarly, scotopic b-wave amplitudes were appropriately 3- and 2-fold higher in VAR10303-treated P30 (*P* < 0.01) and P42 (*P* < 0.05) rd10 mice than their age-matched rd10 controls, respectively (Figs. 2D–E), suggesting a significant rescue of retinal function with VAR10303 treatment.

To evaluate spatial visual performance in rd10 animals treated with VK28 or VAR10303, we measured mouse optomotor responses to moving gratings of different spatial frequencies at P26 (Fig. 3A). We found that photopic visual acuity in VAR10303-treated rd10 mice was significantly better

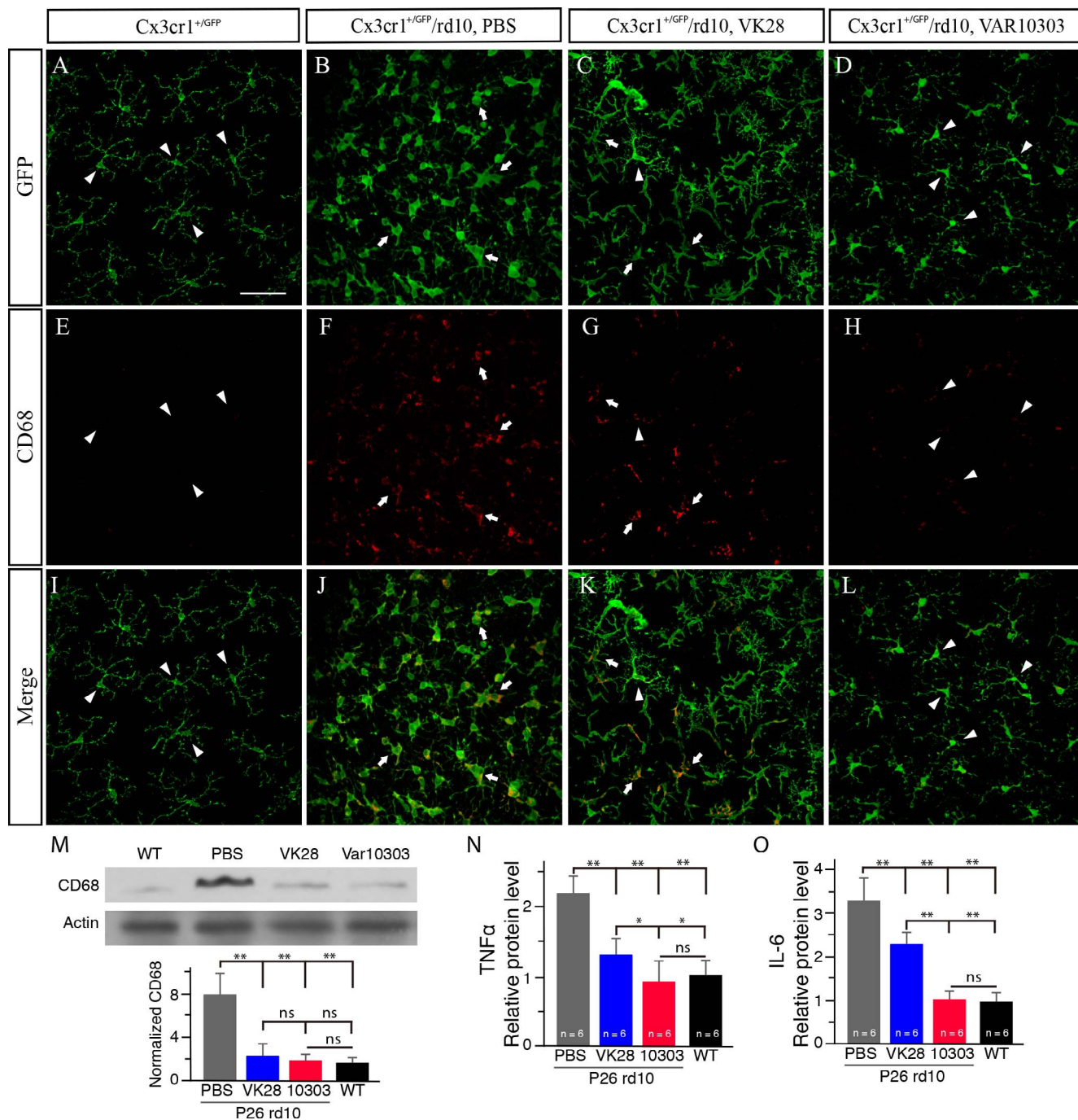


**FIGURE 4.** VK28 and VAR10303 reduced microglia activation and productions of proinflammatory mediators in the rd10 mouse retina. Microglia maintain a ramified morphology in Cx3cr1<sup>+/GFP</sup> control mouse retinas (A), and CD68 staining is undetectable (E, I) (arrowheads). Microglia show amoeboid morphology with few processes and rounded cell bodies in PBS-treated P26 Cx3cr1<sup>+/GFP</sup>/rd10 retinas (B) (arrows), and CD68 staining is intense and widespread (F, J) (arrows). VK28 and VAR10303 treatments preserved the ramified appearance of microglia in Cx3cr1<sup>+/GFP</sup>/rd10 retinas (C, D) (arrowheads), and reduced CD68 immunoreactivity (G, H, K, L) (arrows). (M) Western blotting analysis and densitometry of CD68 protein expressions from PBS-, VK28-, and VAR10303-treated P26rd10 mouse retinas and WT mouse retinas (n = 8–12 in each group). (N–O) ELISA analysis of TNF-α (N) and IL-6 (O) protein expression levels in the retina of WT and PBS-, VK28- and VAR10303-treated rd10 mice. Results are presented as means ± SDs and were analyzed using the Student's *t*-test. \**P* < 0.05, \*\**P* < 0.01; ns, not significant. Scale bar: 50 μm.

than that in PBS-treated rd10 controls (*P* < 0.01; Fig. 3B). However, the visual acuity in VAR10303-treated rd10 mice was still poorer than that in WT control mice (*P* < 0.01; Fig. 3B), indicating partial rescue of retinal function by VAR10303 treatment. We did not observe improved visual performance in VK28-treated rd10 mice at P26, which was consistent with ERG results in the same age of VK28-treated rd10 mice.

### VK28 and VAR10303 Suppressed Microglia Activation in the rd10 Retina

Microglial activation has been shown to contribute to the pathogenesis in RP retinas.<sup>20–23</sup> We investigated whether VK28 and VAR10303 treatments suppressed microglial activation in the rd10 retina. Microglia have a ramified appearance in Cx3cr1<sup>+/GFP</sup> control mouse retinas (Fig. 4A, arrowheads). A

gradual morphologic change in microglia from a ramified appearance into an amoeboid shape with retracted processes and rounded cell bodies was observed in the PBS-treated Cx3cr1<sup>+/GFP</sup>/rd10 retina (Fig. 4B, arrows). However, microglia maintained ramified morphology in VK28- and VAR10303-treated Cx3cr1<sup>+/GFP</sup>/rd10 mouse retinas (Figs. 4C, 4D, arrowheads). To confirm the status of microglial activation, we performed CD68 staining, a marker for microglia activation. CD68 immunoreactivity was undetectable in Cx3cr1<sup>+/GFP</sup> control mouse retinas (Figs. 4E, 4I), while CD68 immunoreactivity was widespread and intense in the rd10 retina (Figs. 4F, 4J). VK28 and VAR10303 treatments led to reduction of CD68 immunoreactivity (Figs. 4G, 4H, 4K, 4L), which was further confirmed by Western blotting analysis (Fig. 4M).

Moreover, we measured the expression levels of the inflammatory mediator TNF- $\alpha$  and IL-6 by ELISA analysis. Compared with WT retinas, TNF- $\alpha$  and IL-6 protein expressions increased approximately by 2- and 3-fold in rd10 mouse retinas, respectively ( $P < 0.01$ ; Figs. 4N, 4O). However, VK28 and VAR10303 treatments markedly reduced the protein expression levels of TNF- $\alpha$  and IL-6 ( $P < 0.01$ ; Figs. 4N, 4O), indicating attenuation of neuroinflammation in drug-treated rd10 retinas.

Furthermore, we sought to gain more insight into mechanisms underlying the suppression of microglial activation by VK28 and VAR10303 treatments. Nuclear-factor kappa B is known to induce the transcription of proinflammatory genes.<sup>45,46</sup> Nuclear factor- $\kappa$ B is bound to I $\kappa$ B in the cytoplasm under normal physiological conditions. Under pathologic conditions, I $\kappa$ B is phosphorylated and degraded, leading to activation of NF- $\kappa$ B. Subsequently, NF- $\kappa$ B is translocated to the nucleus and activates the expression of proinflammatory cytokine genes. We thus studied the expression level of NF- $\kappa$ B in the nucleus, and I $\kappa$ B in the cytoplasm. Nuclear factor- $\kappa$ B exists in several dimeric forms, predominantly the p50/p65 heterodimer. ELISA analysis demonstrated a significant increase in phosphorylated-NF- $\kappa$ B p65 in PBS-treated rd10 retinas ( $P < 0.01$ ; Fig. 5A), but the increases were significantly counteracted by VK28 and VAR10303 treatments, leading to a significant reduction in the expression levels of NF- $\kappa$ B p65 in rd10 retinas (Fig. 5A). Meanwhile, Western blotting analysis showed that phosphorylated-I $\kappa$ B $\alpha$  (p-I $\kappa$ B $\alpha$ ) expression increased by 4.2-fold in PBS-treated rd10 retinas, compared with WT retinas (Fig. 5B). After VK28 and VAR10303 treatments, p-I $\kappa$ B $\alpha$  expression levels were decreased by 1.4- and 2.6-fold in rd10 mouse retinas, respectively, when compared with PBS-treated rd10 retinas (Fig. 5B). Conversely, I $\kappa$ B $\alpha$  protein expression decreased by 10-fold in PBS-treated rd10 mice (Fig. 5C), compared with WT retinas. On the other hand, I $\kappa$ B $\alpha$  protein levels increased by 7.9- and 1.6-fold in VAR10303- and VK28-treated rd10 retinas, respectively (Fig. 5C). Taken together, our data showed that reduction of proinflammatory mediators by VK28 and VAR10303 treatments in the rd10 retina correlated to downregulation of NF- $\kappa$ B.

### The Mechanisms of Actions of VK28 and VAR10303 in the rd10 Retina

To further explore the mechanisms underlying the rescue of cone photoreceptors, we evaluated the several mechanisms that are previously reported to contribute to photoreceptor cell death in RP. Altered iron metabolism is implicated in retinal degenerations including RP.<sup>14,47</sup> We thus performed Western blotting analysis to assess the expression level of the iron metabolism-related protein transferrin. Transferrin expression have been shown to increase during the course of retinal degeneration in rd10 mice.<sup>14</sup> We have confirmed the upregulation of transferrin expression in rd10 retinas (Fig. 6A).

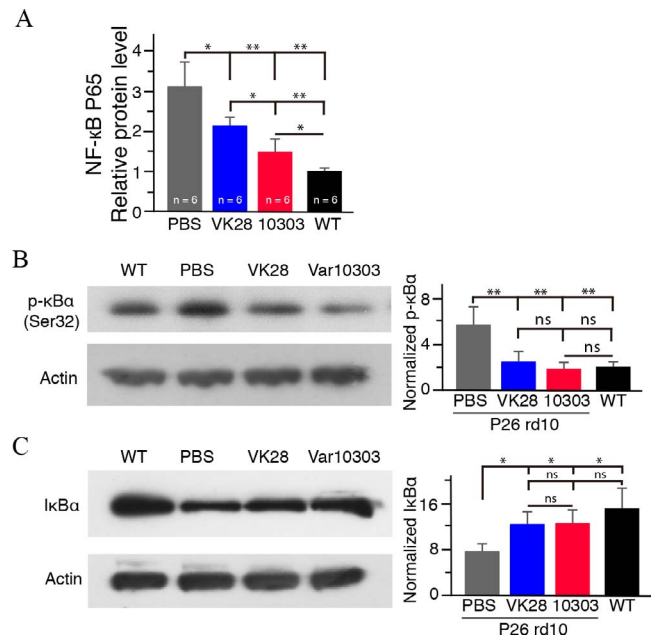


**FIGURE 5.** VK28 and VAR10303 downregulated proinflammatory molecules in the rd10 mouse retina. (A) Nuclear factor- $\kappa$ B p65 protein expression levels in the retina of WT, and PBS-, VK28- and VAR10303-treated rd10 mice by ELISA. (B, C) Western blotting analysis and densitometry of phospho-I $\kappa$ B $\alpha$  (B) and I $\kappa$ B $\alpha$  (C) expression levels in the retina of P26 WT mice, and PBS-, VK28- and VAR10303-treated P26 rd10 mice ( $n = 8-12$  in each group).  $\beta$ -actin levels were used as loading controls. Results are presented as means  $\pm$  SDs and were analyzed using the Student's  $t$ -test. \* $P < 0.05$ , \*\* $P < 0.01$ ; ns, not significant.

Systemic administration of VK28 or VAR10303 significantly downregulated transferrin expression in rd10 retinas (Fig. 6A), indicating a possible protective therapeutic approach against iron overload-induced photoreceptor degeneration.

Moreover, oxidative stress causes photoreceptor dysfunction and cell death in RP mouse models.<sup>7,13</sup> We measured several biomarkers of oxidative stress, including MDA, reduced GSH, GSSG, and GSH/GSSG. Malondialdehyde is a common lipid peroxidation product that accumulates in many pathophysiological processes. We found that MDA expression increased approximately by 2-fold in rd10 retinas compared with WT retinas ( $P < 0.01$ ; Fig. 6B). VK28 and VAR10303 treatments significantly reduced the expression levels of MDA in rd10 retinas compared with PBS-treated rd10 retinas ( $P < 0.01$ ; Fig. 6B). The GSH/GSSG status is commonly used in measuring oxidative stress status, and a reduction in GSH/GSSG ratio reflects a reduced antioxidant capacity. A significant reduction in GSH/GSSG ratio was observed in rd10 retinas, compared with WT retinas ( $P < 0.01$ ; Fig. 6C), and VAR10303 and VK28 treatments significantly increased the GSH/GSSG ratio ( $P < 0.01$ ; Fig. 6C), indicating an increased antioxidant capacity.

Furthermore, we investigated whether VAR10303 and VK28 regulated the apoptotic pathway. Caspases are a family of genes important for the apoptotic response. We evaluated the expression levels of the initiator caspase, caspase-8, and the effector caspases, caspases-3/7. We found that the protein expression levels of caspase-3/7 and -8 were significantly higher in PBS-treated rd10 retinas than in WT controls ( $P < 0.01$ ; Figs. 6D, 6E). Treatments with VK28 and VAR10303 significantly decreased the protein levels of caspase-3/7 and -8 in rd10 retinas ( $P < 0.01$ ; Figs. 6D, 6E).

Hypoxia-inducible factor 1 $\alpha$ , an oxygen-sensitive transcriptional activator, plays an important role in cellular response to systemic oxygen levels in mammals. We found that HIF-1 $\alpha$  was

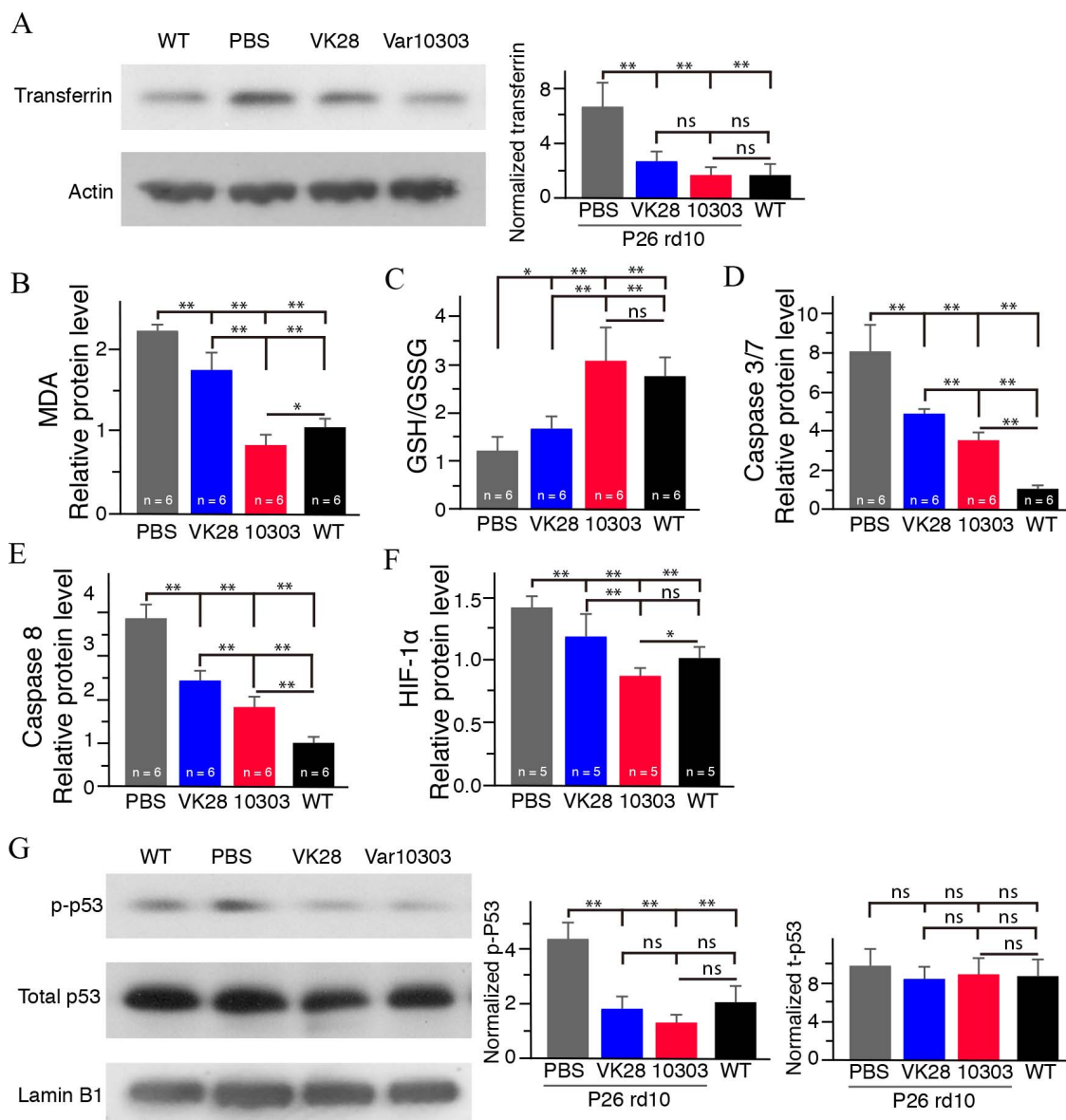


**FIGURE 6.** VK28 and VAR10303 downregulated oxidative-related enzymes and proapoptotic molecules in the rd10 mouse retina. (A) Western blot analysis and densitometry of transferrin expression in the retina of WT, and PBS-, VK28- and VAR10303-treated P26 rd10 mice ( $n = 8-12$  in each group). (B-F) ELISA analysis of MDA (B), GSH and GSSG (C), caspase-3/7 (D), caspase-8 (E), and HIF-1 $\alpha$  (F) protein expression levels in the retina of WT, PBS-, VK28-, and VAR10303-treated rd10 mice. (G) Western blot analysis and densitometry of total p53 and p-p53 protein expressions in the retina of WT, PBS-, VK28-, and VAR10303-treated rd10 mice ( $n = 8-12$  in each group). Results are presented as means  $\pm$  SDs and were analyzed using the Student's  $t$ -test. \* $P < 0.05$ , \*\* $P < 0.01$ ; ns, not significant.

upregulated in rd10 retinas (Fig. 6F), and the increases were counteracted by VAR10303 and VK28 treatments ( $P < 0.01$ ; Fig. 6F). The key tumor suppressor protein p53, a downstream target of HIF-1 $\alpha$ , has a diverse range of functions, including the ability to promote apoptosis.<sup>48</sup> Western blotting analysis showed that total p53 protein level in the nucleus was comparable among WT retinas, PBS-, VK28- and VAR10303-treated rd10 mouse retinas (Fig. 6G). However, phosphorylated-p53 (p-p53) expression level increased in rd10 retinas compared with WT retinas (Fig. 6G). Treatments by VK28 and VAR10303 dramatically decreased p-p53 protein levels in rd10 retinas (Fig. 6G). These findings indicated that downregulation of nuclear p53 was likely to be the mechanism underlying reduced apoptosis in photoreceptors in the rd10 retina after VK28 and VAR10303 treatments.

Taken together, our data suggested that VK28 and VAR10303 exerted protective effects likely through regulation of iron bioavailability, oxidative stress, and photoreceptor apoptosis, leading to partial rescue of photoreceptors in rd10 mice.

## DISCUSSION

In this study, we investigate the effects of two iron-chelating drugs on the rescue of cone photoreceptors in the rd10 mouse model of RP. We demonstrated a significant rescue of the structure and function of cone photoreceptors by the two iron-chelating drugs, VK28 and VAR10303, for extended periods, during a time that they would ordinarily degenerate in rd10 mouse retina. Moreover, we showed that the two compounds

exerted their effects by altering the profile of cone degeneration through the possible synergism of anti-inflammatory, antioxidant, and antiapoptotic mechanisms of actions in the rd10 retina.

Neuroinflammation is an underlying component of a diverse range of chronic neurodegenerative disorders.<sup>49,50</sup> Microglia activation has been reported to be associated with photoreceptor degeneration in mouse models of RP and human RP.<sup>20-23</sup> We found that VAR10303 and VK28 dramatically reduced microglia activation, and subsequently diminished the production of proinflammatory cytokines including CD68, TNF- $\alpha$ , and IL-6 $\beta$  in the rd10 retina. Moreover, we demonstrated that downregulation of NF- $\kappa$ B was likely to be the mechanism by which the proinflammatory mediators were downregulated. Consistently, increased activity of NF- $\kappa$ B and its neurotoxic role in photoreceptor cell death have been previously reported in the rd1 mouse model of RP.<sup>51</sup>

Iron-associated oxidative stress plays an important pathogenic role in neurodegenerative diseases including AMD and RP.<sup>14,52-54</sup> Similarly, iron accumulation and increased expression of iron-regulating protein transferrin were shown in rd10 retinas.<sup>14,55</sup> We have demonstrated that VAR10303 and VK28 downregulated transferrin expression in rd10 retinas, which might oppose iron overload-induced cone degeneration.

Moreover, VAR10303 and VK28 counteracted oxidative stress by restoring antioxidant enzymes and limiting iron bioavailability in rd10 retinas, resulting in attenuation of oxidative stress injury in the rd10 retinas. The findings are consistent with our previous observation that two compounds are capable of chelating iron and suppressing iron-induced oxidative stress, and subsequently attenuating neuronal loss in Alzheimer's and Parkinson's diseases animal models.<sup>24,27,28,56</sup> In accordance, a recent study demonstrated a reduction in retinal oxidative stress by the iron chelator desferrioxamin in rd10 mouse retina.<sup>16</sup>

Furthermore, it has been shown that caspase-dependent upregulation is involved in photoreceptor cell death in RP.<sup>12,57</sup> Indeed, the upregulation of caspase-3 has been reported in the rd1 mouse model of RP.<sup>43,58</sup> Administration of VAR10303 and VK28 resulted in a significant reduction of caspase-3/7 and -8 protein levels, which might reflect the possible effect of the compounds on photoreceptor apoptosis. Consistent with current findings, we have previously shown that VAR10303 and VK28 significantly downregulated proapoptotic proteins in the animal models of Alzheimer's and Parkinson's diseases.<sup>27,28,59,60</sup> Moreover, HIF-1 $\alpha$  upregulation is observed during photoreceptor degeneration in several mouse models of RP.<sup>11</sup> Downregulation of HIF-1 $\alpha$  and p53 that we observed in the present study was probably the mechanisms underlying reduced apoptosis in photoreceptors in the rd10 retina.

Finally, VK28 and VAR10303 also protected rods from degeneration in the rd10 retina. The partial rescue of rod photoreceptor cells might subsequently improve the survival of cones. Indeed, previous studies suggested that rod-derived cone viability factor (RdCVF) maintained the viability and function of cones in the retina, and mice that lack RdCVF showed a gradual loss of photoreceptors.<sup>61</sup> Therefore, the rescue of rods by VK28 and VAR10303 might partially account for the survival of cones in the present study.

In summary, we demonstrated that VK28 and VAR10303 provided significant rescue of cone photoreceptors in RP mice, and the neuroprotective effects of the two compounds on cone photoreceptors correlated to inhibition of microglial activation, oxidative stress, and apoptosis. Therefore, iron-chelation therapeutic strategy may hold great prospects for an effective treatment of RP.

## Acknowledgments

Supported by grants from the General Research Fund from the Hong Kong Research Grants Council (GRF/RGC; BL; Hong Kong, SAR), Health and Medical Research Fund (HMRF; BL; Hong Kong, SAR), National Natural Science Foundation of China (31600839; BP; Hong Kong, SAR), Guangdong Innovative and Entrepreneurial Research Team Program (2013S046; BP; Shenzhen, Guangdong, China), and Shenzhen Peacock Plan (BP; Shenzhen, Guangdong, China), National Key R&D Program of China (2017YFC0111202; BP; Shenzhen, Guangdong, China), Shenzhen Science and Technology Research Program (JCYJ20170307171222692; BP; Shenzhen, Guangdong, China).

Disclosure: **K. Wang**, None; **B. Peng**, None; **J. Xiao**, None; **O. Weinreb**, None; **M.B.H. Youdim**, Youdim Pharmaceuticals Ltd. (I, S); **B. Lin**, None

## References

- Hartong DT, Berson EL, Dryja TP. Retinitis pigmentosa. *Lancet*. 2006;368:1795-1809.
- Bramall AN, Wright AF, Jacobson SG, McInnes RR. The genomic, biochemical, and cellular responses of the retina in inherited photoreceptor degenerations and prospects for the treatment of these disorders. *Ann Rev Neurosci*. 2010;33:441-472.
- Oyster CW. *The Human Eye Structure and Function*. Sunderland: Sinauer; 1999.
- Pacione LR, Szego MJ, Ikeda S, Nishina PM, McInnes RR. Progress toward understanding the genetic and biochemical mechanisms of inherited photoreceptor degenerations. *Annu Rev Neurosci*. 2003;26:657-700.
- Ait-Ali N, Fridlich R, Millet-Puel G, et al. Rod-derived cone viability factor promotes cone survival by stimulating aerobic glycolysis. *Cell*. 2015;161:817-832.
- Bennett J, Tanabe T, Sun D, et al. Photoreceptor cell rescue in retinal degeneration (rd) mice by in vivo gene therapy. *Nat Med*. 1996;2:649-654.
- Komeima K, Rogers BS, Lu L, Campochiaro PA. Antioxidants reduce cone cell death in a model of retinitis pigmentosa. *Proc Natl Acad Sci U S A*. 2006;103:11300-11305.
- MacLaren RE, Pearson RA, MacNeil A, et al. Retinal repair by transplantation of photoreceptor precursors. *Nature*. 2006;444:203-207.
- Wang X, Zhao L, Zhang Y, et al. Tamoxifen provides structural and functional rescue in murine models of photoreceptor degeneration. *J Neurosci*. 2017;37:3294-3310.
- Yu W, Mookherjee S, Chaitankar V, et al. Nrl knockdown by AAV-delivered CRISPR/Cas9 prevents retinal degeneration in mice. *Nat Commun*. 2017;8:14716.
- Punzo C, Kornacker K, Cepko CL. Stimulation of the insulin/mTOR pathway delays cone death in a mouse model of retinitis pigmentosa. *Nat Neurosci*. 2009;11:44-52.
- Wright AF, Chakarova CF, Abd El-Aziz MM, Bhattacharya SS. Photoreceptor degeneration: genetic and mechanistic dissection of a complex trait. *Nat Rev Genet*. 2010;11:273-284.
- Komeima K, Rogers BS, Campochiaro PA. Antioxidants slow photoreceptor cell death in mouse models of retinitis pigmentosa. *J Cell Physiol*. 2007;213:809-815.
- Deleon E, Lederman M, Berenstein E, Meir T, Chevion M, Chowers I. Alteration in iron metabolism during retinal degeneration in rd10 mouse. *Invest Ophthalmol Vis Sci*. 2009;50:1360-1365.
- He X, Hahn P, Iacovelli J, et al. Iron homeostasis and toxicity in retinal degeneration. *Prog Retin Eye Res*. 2007;26:649-673.
- Obolensky A, Berenshtein E, Lederman M, et al. Zinc-desferrioxamine attenuates retinal degeneration in the rd10

- mouse model of retinitis pigmentosa. *Free Radic Biol Med*. 2011;51:1482-1491.
17. Song D, Song Y, Hadziahmetovic M, Zhong Y, Dunaief JL. Systemic administration of the iron chelator deferiprone protects against light-induced photoreceptor degeneration in the mouse retina. *Free Radic Biol Med*. 2012;53:64-71.
  18. Karlstetter M, Scholz R, Rutar M, Wong WT, Provis JM, Langmann T. Retinal microglia: just bystander or target for therapy? *Prog Retin Eye Res*. 2015;45:30-57.
  19. Langmann T. Microglia activation in retinal degeneration. *J Leukoc Biol*. 2007;81:1345-1351.
  20. Gupta N, Brown KE, Milam AH. Activated microglia in human retinitis pigmentosa, late-onset retinal degeneration, and age-related macular degeneration. *Exp Eye Res*. 2003;76:463-471.
  21. Zeiss CJ, Johnson EA. Proliferation of microglia, but not photoreceptors, in the outer nuclear layer of the rd-1 mouse. *Invest Ophthalmol Vis Sci*. 2004;45:971-976.
  22. Zeng HY, Zhu XA, Zhang C, Yang LP, Wu LM, Tso MO. Identification of sequential events and factors associated with microglial activation, migration, and cytotoxicity in retinal degeneration in rd mice. *Invest Ophthalmol Vis Sci*. 2005;46:2992-2999.
  23. Peng B, Xiao J, Wang K, So KF, Tipoe GL, Lin B. Suppression of microglial activation is neuroprotective in a mouse model of human retinitis pigmentosa. *J Neurosci*. 2014;34:8139-8150.
  24. Bar-Am O, Amit T, Kupersmidt L, et al. Neuroprotective and neurorestorative activities of a novel iron chelator-brain selective monoamine oxidase-A/monoamine oxidase-B inhibitor in animal models of Parkinson's disease and aging. *Neurobiol Aging*. 2015;36:1529-1542.
  25. Golko-Perez S, Amit T, Youdim MB, Weinreb O. A novel iron chelator-radical scavenger ameliorates motor dysfunction and improves life span and mitochondrial biogenesis in SOD1G93A ALS mice. *Neurotox Res*. 2017;31:230-244.
  26. Golko-Perez S, Amit T, Youdim MB, Weinreb O. Beneficial effects of multitarget iron chelator on central nervous system and gastrocnemius muscle in SOD1(G93A) transgenic ALS mice. *J Mol Neurosci*. 2016;59:504-510.
  27. Shachar DB, Kahana N, Kampel V, Warshawsky A, Youdim MB. Neuroprotection by a novel brain permeable iron chelator, VK-28, against 6-hydroxydopamine lesion in rats. *Neuropharmacology*. 2004;46:254-263.
  28. Zheng H, Gals S, Weiner LM, et al. Novel multifunctional neuroprotective iron chelator-monoamine oxidase inhibitor drugs for neurodegenerative diseases: in vitro studies on antioxidant activity, prevention of lipid peroxide formation and monoamine oxidase inhibition. *J Neurochem*. 2005;95:68-78.
  29. Zhu W, Xie W, Pan T, et al. Prevention and restoration of lactacystin-induced nigrostriatal dopamine neuron degeneration by novel brain-permeable iron chelators. *FASEB J*. 2007;21:3835-3844.
  30. Xiao J, Ching YP, Liang EC, Nanji AA, Fung ML, Tipoe GL. Garlic-derived S-allylmercaptocysteine is a hepato-protective agent in non-alcoholic fatty liver disease in vivo animal model. *Eur J Nutr*. 2013;52:179-191.
  31. Guo R, Lin B, Pan JF, et al. Inhibition of caspase-9 aggravates acute liver injury through suppression of cytoprotective autophagy. *Sci Rep*. 2016;6:32447.
  32. Rossger K, Charpin-El-Hamri G, Fussenegger M. A closed-loop synthetic gene circuit for the treatment of diet-induced obesity in mice. *Nat Commun*. 2013;4:2825.
  33. Pauls E, Nanda SK, Smith H, Toth R, Arthur JSC, Cohen P. Two phases of inflammatory mediator production defined by the study of IRAK2 and IRAK1 knock-in mice. *J Immunol*. 2013;191:2717-2730.
  34. Wang K, Xiao J, Peng B, et al. Retinal structure and function preservation by polysaccharides of wolfberry in a mouse model of retinal degeneration. *Sci Rep*. 2014;4:7601.
  35. da Silva RP, Gordon S. Phagocytosis stimulates alternative glycosylation of macrofialin (mouse CD68), a macrophage-specific endosomal protein. *Biochem J*. 1999;338(Pt 3):687-694.
  36. Janda E, Lehmann K, Killisch I, et al. Ras and TGF[beta] cooperatively regulate epithelial cell plasticity and metastasis: dissection of Ras signaling pathways. *J Cell Biol*. 2002;156:299-313.
  37. Doiron K, Goyon V, Coyaud E, Rajapakse S, Raught B, McBride HM. The dynamic interacting landscape of MAPL reveals essential functions for SUMOylation in innate immunity. *Sci Rep*. 2017;7:107.
  38. Zhu J, Sammons MA, Donahue G, et al. Gain-of-function p53 mutants co-opt chromatin pathways to drive cancer growth. *Nature*. 2015;525:206-211.
  39. Patel A, Yamashita N, Ascaño, et al. RCAN1 links impaired neurotrophin trafficking to aberrant development of the sympathetic nervous system in Down syndrome. *Nat Commun*. 2015;6:10119.
  40. Chang B, Hawes NL, Hurd RE, Davission MT, Nusinowitz S, Heckenlively JR. Retinal degeneration mutants in the mouse. *Vision Res*. 2002;42:517-525.
  41. McLaughlin ME, Sandberg MA, Berson EL, Dryja TP. Recessive mutations in the gene encoding the beta-subunit of rod phosphodiesterase in patients with retinitis pigmentosa. *Nat Genet*. 1993;4:130-134.
  42. Chen M, Wang K, Lin B. Development and degeneration of cone bipolar cells are independent of cone photoreceptors in a mouse model of retinitis pigmentosa. *PLoS One*. 2012;7:e44036.
  43. Gargini C, Terzibasi E, Mazzoni F, Strettoi E. Retinal organization in the retinal degeneration 10 (rd10) mutant mouse: a morphological and ERG study. *J Comp Neurol*. 2007;500:222-238.
  44. Jeon CJ, Strettoi E, Masland RH. The major cell populations of the mouse retina. *J Neurosci*. 1998;18:8936.
  45. Li Q, Verma IM. NF-kappaB regulation in the immune system. *Nat Rev Immunol*. 2002;2:725-734.
  46. Vallabhapurapu S, Karin M. Regulation and function of NF-kappaB transcription factors in the immune system. *Ann Rev Immunol*. 2009;27:693-733.
  47. Yefimova MG, Jeanny JC, Keller N, et al. Impaired retinal iron homeostasis associated with defective phagocytosis in Royal College of Surgeons rats. *Invest Ophthalmol Vis Sci*. 2002;43:537-545.
  48. Vousden KH, Ryan KM. p53 and metabolism. *Nat Rev Cancer*. 2009;9:691-700.
  49. Glass CK, Saijo K, Winner B, Marchetto MC, Gage FH. Mechanisms underlying inflammation in neurodegeneration. *Cell*. 2010;140:918-934.
  50. Yong VW, Rivest S. Taking advantage of the systemic immune system to cure brain diseases. *Neuron*. 2009;64:55-60.
  51. Zeng HY, Tso MO, Lai S, Lai H. Activation of nuclear factor-kappaB during retinal degeneration in rd mice. *Mol Vis*. 2008;14:1075-1080.
  52. Hahn P, Qian Y, Dentchev T, et al. Disruption of ceruloplasmin and hephaestin in mice causes retinal iron overload and retinal degeneration with features of age-related macular degeneration. *Proc Natl Acad Sci U S A*. 2004;101:13850-13855.
  53. Rouault TA. Iron metabolism in the CNS: implications for neurodegenerative diseases. *Nat Rev Neurosci*. 2013;14:551-564.

54. Zecca L, Youdim MB, Riederer P, Connor JR, Crichton RR. Iron, brain ageing and neurodegenerative disorders. *Nat Rev Neurosci.* 2004;11:863-873.
55. Picard E, Jonet L, Sergeant C, et al. Overexpressed or intraperitoneally injected human transferrin prevents photoreceptor degeneration in rd10 mice. *Mol Vis.* 2010;16:2612-2625.
56. Kupersmidt L, Amit T, Bar-Am O, Youdim MB, Weinreb O. The novel multi-target iron chelating-radical scavenging compound M30 possesses beneficial effects on major hallmarks of Alzheimer's disease. *Antioxid Redox Signal.* 2012;17:860-877.
57. Sancho-Pelluz J, Arango-Gonzalez B, Kustermann S, et al. Photoreceptor cell death mechanisms in inherited retinal degeneration. *Mol Neurobiol.* 2008;38:253-269.
58. Zeiss CJ, Neal J, Johnson EA. Caspase-3 in postnatal retinal development and degeneration. *Invest Ophthalmol Vis Sci.* 2004;45:964-970.
59. Kupersmidt L, Weinreb O, Tamar A, Youdim M. Protective effects of the novel multi-target iron chelator /monoamine oxidase inhibitor drug, VAR, on age-related neurodegeneration: regulation of BDNF/CREB signaling. *J Mol Neurosci.* 2013;51:S65.
60. Weinreb O, Bar-Am O, Amit T, Chillag-Talmor O, Youdim MB. Neuroprotection via pro-survival protein kinase C isoforms associated with Bcl-2 family members. *FASEB J.* 2004;18:1471-1473.
61. Léveillard T, Sahel JA. Rod-derived cone viability factor for treating blinding diseases: From clinic to redox signaling. *Sci Transl Med.* 2010;2:26ps16.